OECD MCCI Project

Small-Scale Water Ingression and Crust Strength Tests (SSWICS)

SSWICS-6 Test Data Report: Thermal Hydraulic Results

Rev. 0 March 22, 2004

by:

S. Lomperski, M. T. Farmer, D. Kilsdonk, B. Aeschlimann

Nuclear Engineering Division
Argonne National Laboratory
9700 S. Cass Avenue
Argonne, IL 60439
USA

Table of Contents

List of Plots

1. Introduction

The Melt Attack and Coolability Experiments (MACE) program at Argonne National Laboratory addressed the issue of the ability of water to cool and thermally stabilize a molten core/concrete interaction (MCCI) when the reactants are flooded from above. These tests provided data regarding the nature of corium interactions with concrete, the heat transfer rates from the melt to the overlying water pool, and the role of noncondensable gases in the mixing processes that contribute to melt quenching. However, due to the integral nature of these tests, several questions regarding the crust freezing behavior could not be adequately resolved. These questions include:

1) To what extent does water ingression into the crust increase the melt quench rate above the conduction-limited rate and how is this affected by melt composition and system pressure?
2) What is the fracture strength of the corium crust when subjected to a thermal-mechanical load and how does it depend upon the melt composition?

A series of separate-effects experiments are being conducted to address these issues. The first employs an apparatus designed to measure the quench rate of a pool of corium (~ϕ30 cm; up to 20 cm deep). The main parameter to be varied in these quench tests is the melt composition since it is thought to have a critical influence on the crust cracking behavior which, in turn, alters quench rate. The issue of crust strength is being addressed with a second apparatus designed to mechanically load the crust produced by the quench tests. This apparatus measures the fracture strength of the crust while it is either at room temperature or above, the latter state being achieved with a heating element placed below the crust. The two apparatuses used to measure the melt quench rate and crust strength are jointly referred to as SSWICS (Small-Scale Water Ingression and Crust Strength).

This report describes results of the sixth water ingression test, designated SSWICS-6. This test investigated the quenching behavior of a fully oxidized PWR corium melt containing 15 wt% siliceous concrete at a system pressure of 1 bar absolute. The report includes a description of the test apparatus, the instrumentation used, plots of the recorded data, and some rudimentary data reduction to obtain an estimate of the heat flux from the corium to the overlying water pool.

2. System Description

2.1 Test Apparatus

The SSWICS reaction vessel (RV) has been designed to hold up to 100 kg of melt at an initial temperature of 2500°C. The RV lower plenum consists of a 67.3 cm long, 45.7 cm (18") outer diameter carbon steel pipe (fig. 2.1). The pipe is insulated from the melt by a 6.4 cm thick layer of cast MgO, which is called the "liner". The selected pipe and insulation dimensions result in a melt diameter of about 30 cm and a surface area of 707 cm^2. The melt depth at the maximum charge of 100 kg is about 20 cm.

The RV lower flange is insulated with a 6.4 cm thick slab of cast MgO (the "basemat") that spans the entire inner diameter of the pipe. The basemat and liner form the crucible containing

the corium. This particular geometry was chosen to facilitate removal of the basemat for the crust strength measurement tests. Corium has a tendency to bond with the MgO insulation and this design allows one to detach the basemat from the liner without damaging the crust.

The basemat lies beneath a 1.3 cm thick cast ZrO_2 plate. The ZrO_2 is added because of its exceptionally low thermal conductivity at high temperature (~1 W/m°C, versus ~10 for MgO at 2000°C). Despite its low thermal conductivity, the ZrO_2 is not used as the primary insulator to protect the flange because of its poor thermal shock resistance. To protect the cast ZrO_2 plate from the initial thermal shock following thermite ignition, a disk of low-density ZrO_2 board is set on top of the cast plate. This material is not structurally robust and serves as a sacrificial layer that absorbs the initial thermal shock of thermite ignition. Finally, a thin layer (0.25 mm) of tungsten is added in an effort to prevent the erosion of the ZrO_2 that is expected if the corium was allowed to come in direct contact with the low-density board.

The RV upper plenum consists of a second section of pipe with a stainless steel protective liner. Three 10 cm pipes welded near the top of the vessel provide 1) a vent line for the initial surge of hot noncondensable gases generated by the thermite reaction, 2) a pressure relief line with a rupture disk (7.7 bar at 100°C), and 3) an instrument flange for the absolute pressure transmitter that measures the reaction vessel pressure. Four 6 mm (¼") tubes serve as water inlets for melt quenching. A baffle is mounted below the upper flange and the water flow is directed towards the baffle to reduce the momentum of the fluid before it drops down onto the melt. The baffle is also intended to prevent water droplets from being carried up towards the condenser, which would adversely affect the heat flux measurement. A fourth 10 cm pipe welded to the top flange provides an outlet to carry steam from the quenching melt to four cooling coils. The water-cooled coils condense the steam, which is collected within a 200 cm high, 20 cm diameter condensate tank (CT). Figure 2.2 is a schematic that provides an overview of the entire SSWICS melt-quench facility.

2.2 Instrumentation

Instrumentation has been selected to provide all measurements necessary to determine the melt dryout heat flux. Tables 2.1 and 2.2 list the sensors and major valves, respectively.

The critical measurement for these tests is the steaming rate in the RV, which is found indirectly by measuring the rate of condensate collection in the CT. The condensate inventory is measured with a differential pressure sensor, PD-CT, and a time domain reflectometer, L-TDR-CT.

The remaining instrumentation provides supplementary information to further characterize the test conditions. The nomenclature used to identify thermocouples is as follows: TM (temperature within the corium melt), TF (fluid temperature), TG (gas space temperature), TIW (temperature at the inner wall of the liner), TOW (temperature at the outer wall of the liner), TS (structure temperature), H# (height above the bottom of the melt, in mm, ϕ# (angle relative to direction north, in degrees). For example, TIW-H50-ϕ180 is located at the inner wall of the liner, 50 mm above the bottom of the melt and south of the RV axis. Thermocouples within the MgO liner have an added "i" or "o" designation, e.g., TS-MgO-H50-ϕ50-i. These indicate "inner" or "outer" TCs, the latter being further from the edge of the melt (see fig. 2.3). They provide measurements of the local heat flux through the liner, which will be used to estimate the

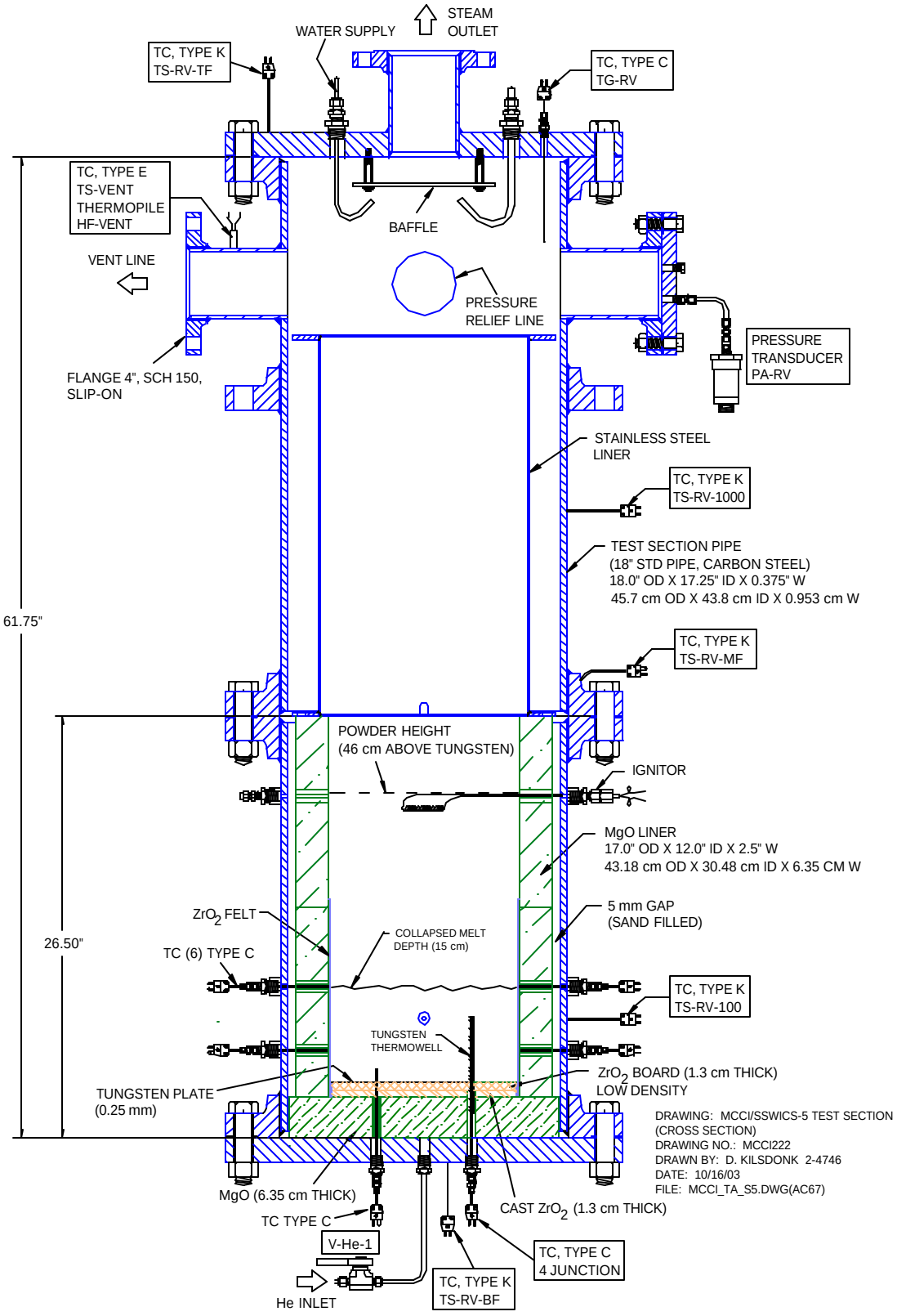

Figure 2.1 Side view of reaction vessel.

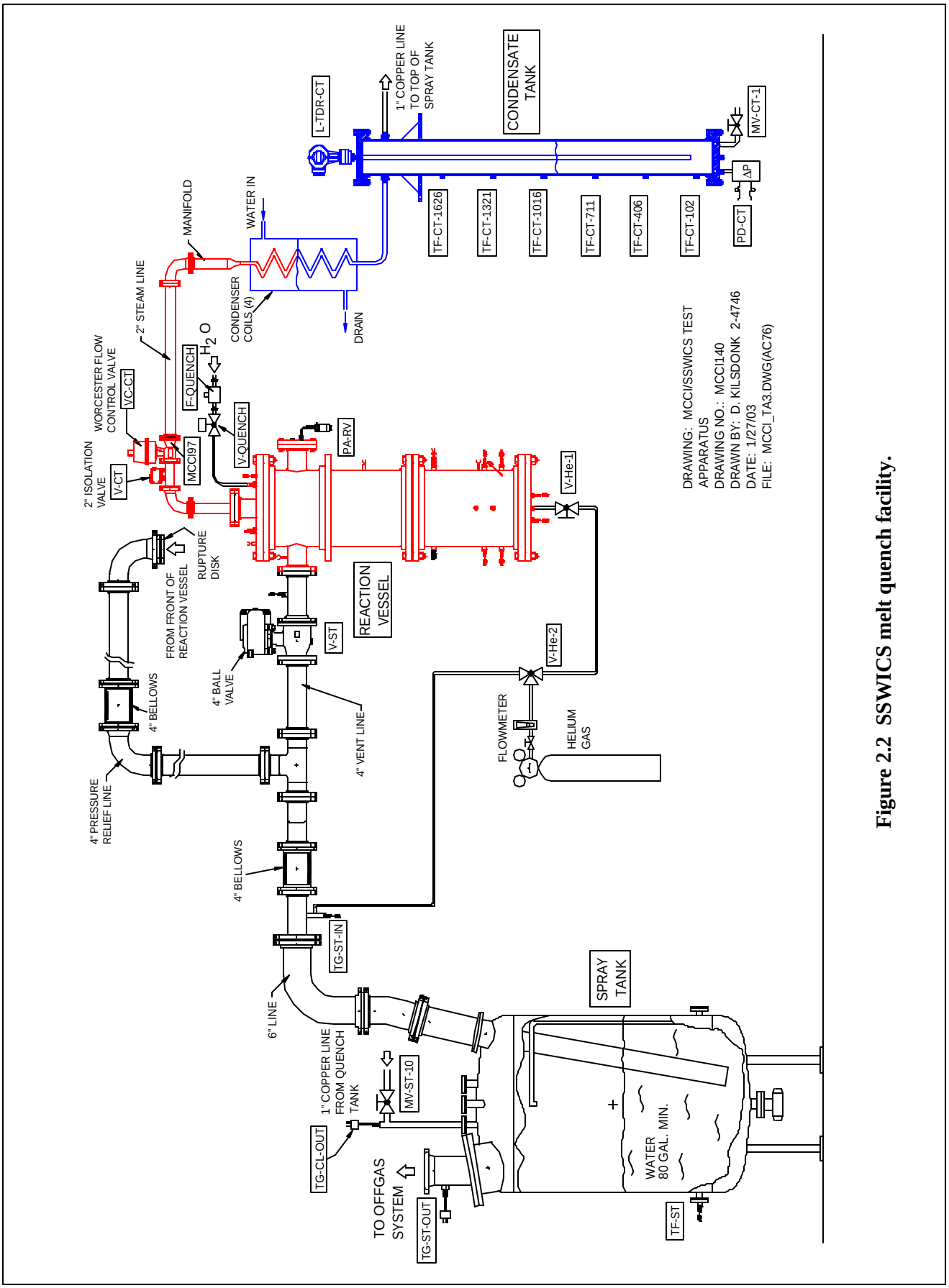

Figure 2.2 SSWICS melt quench facility.

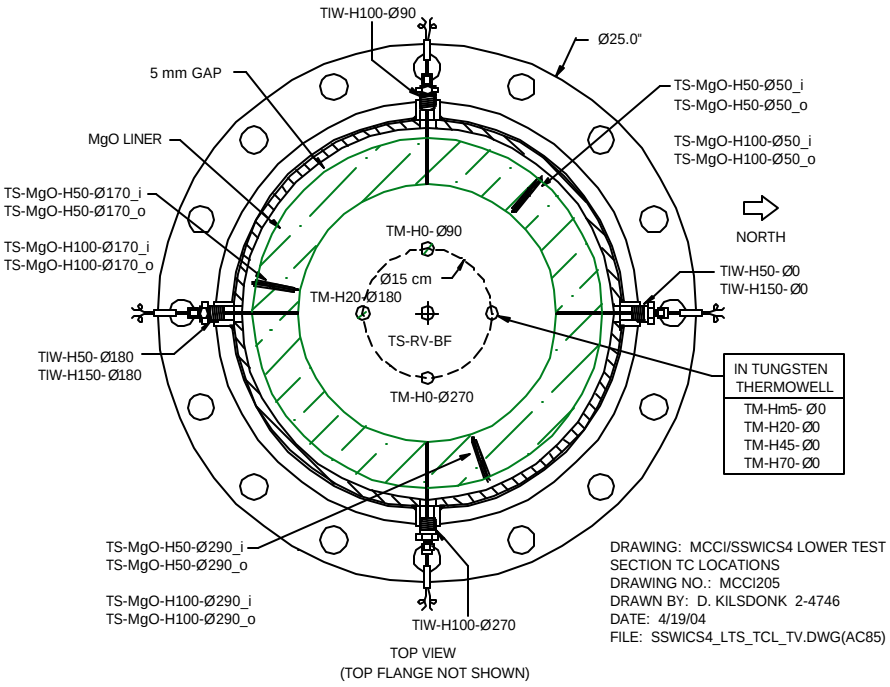

Figure 2.3 Reaction vessel thermocouple locations.

lateral heat losses from the melt. The distance between the inner and outer TCs is 30 mm.

An array of Type-C thermocouples is used to measure the initial temperature of the melt as well as temperatures at the interface between the corium and liner (fig 2.3). These are described further in the paragraphs below.

A multi-junction thermocouple tracks the progress of the quench front through the melt. The thermocouple consists of four sensors and is protected by a tungsten thermowell (6 mm o.d., 150 mm long, 1 mm wall). The designation for the lowest thermocouple inside the tungsten thermowell is unique: TM-Hm5-ϕ0, where the "m5" denotes "minus 5" (5 mm below the bottom of the melt).

Thermocouple TM-H20-ϕ180 is a single-junction sensor in a tantalum sheath with the tip positioned 20 mm above the bottom of the melt. All the melt temperature thermocouples ("TM") are located midway between the center of the melt and the liner inner wall. Thermocouples TM-H0-ϕ90 and TM-H0-ϕ270 are positioned below the low-density ZrO_2 board and near the bottom of the melt. Their function is to detect the arrival of the quench front. The melt is considered quenched when the temperature at the base of the melt reaches the saturation temperature, and this is the basis for terminating the test.

#	Channel	Name	Type	Description	Serial #	Output	Range	Accuracy
0	HPS-0	T-CJ-HPS	AD592 IC	Cold junction compensation sensor.	-	1μA/K	0-70°C	±0.5°C
1	HPS-1	TM-H0-ϕ90	TC type C	Melt temp. at bottom of melt.	-	0-37 mV	0-2320°C	±4.5°C or 1%
2	HPS-2	TM-H0-ϕ270	TC type C	Melt temp. at bottom of melt.	-	0-37 mV	0-2320°C	±4.5°C or 1%
3	HPS-3	TM-H20ϕ180	TC type C	Melt temp. 20 mm above bottom of melt.	-	0-37 mV	0-2320°C	±4.5°C or 1%
4	HPS-4	TM-Hm5-ϕ0	TC type C	Melt temp. 5 mm below bottom of melt (in tungsten thermowell).	-	0-37 mV	0-2320°C	±4.5°C or 1%
5	HPS-5	TM-H20-ϕ0	TC type C	Melt temp. 20 mm above bottom of melt (in tungsten thermowell).	-	0-37 mV	0-2320°C	±4.5°C or 1%
6	HPS-6	TM-H45ϕ0	TC type C	Melt temp. 45 mm above bottom of melt (in tungsten thermowell).	-	0-37 mV	0-2320°C	±4.5°C or 1%
7	HPS-7	TM-H70ϕ0	TC type C	Melt temp. 70 mm above bottom of melt (in tungsten thermowell).	-	0-37 mV	0-2320°C	±4.5°C or 1%
8	HPS-8	TIW-H50-ϕ0	TC type C	Melt temp. at inner sidewall 50 mm above bottom of melt.	-	0-37 mV	0-2320°C	±4.5°C or 1%
9	HPS-9	TIW-H50-ϕ180	TC type C	Melt temp. at inner sidewall 50 mm above bottom of melt.	-	0-37 mV	0-2320°C	±4.5°C or 1%
10	HPS-10	TIW-H100-ϕ90	TC type C	Melt temp. at inner sidewall 100 mm above bottom of melt.	-	0-37 mV	0-2320°C	±4.5°C or 1%
11	HPS-11	TIW-H100-ϕ270	TC type C	Melt temp. at inner sidewall 100 mm above bottom of melt.	-	0-37 mV	0-2320°C	±4.5°C or 1%
12	HPS-12	TIW-H150-ϕ0	TC type C	Melt temp. at inner sidewall 150 mm above bottom of melt.	-	0-37 mV	0-2320°C	±4.5°C or 1%
13	HPS-13	TIW-H150-ϕ180	TC type C	Melt temp. at inner sidewall 150 mm above bottom of melt.	-	0-37 mV	0-2320°C	±4.5°C or 1%
14	HPS-14	Reserve	TC type C	-	-	0-37 mV	0-2320°C	±4.5°C or 1%
15	HPS-15	Reserve	TC type C	-	-	0-37 mV	0-2320°C	±4.5°C or 1%
16	HPS-16	Reserve	TC type C	-	-	0-37 mV	0-2320°C	±4.5°C or 1%
17	HPS-17	Reserve	TC type C	-	-	0-37 mV	0-2320°C	±4.5°C or 1%
18	HPS-18	TG-RV	TC type C	Gas temp. in reaction vessel upper plenum.	-	0-37 mV	0-2320°C	±4.5°C or 1%
19	HPS-19	Reserve	TC type K	-	-	0-50 mV	0-1250°C	± 2.2°C or 0.75%
20	HPS-20	Reserve	TC type K	-	-	0-50 mV	0-1250°C	± 2.2°C or 0.75%
21	HPS-21	Reserve	TC type K	-	-	0-50 mV	0-1250°C	± 2.2°C or 0.75%
22	HPS-22	TS-RV-tf	TC type K	Temperature of RV top flange.	-	0-50 mV	0-1250°C	± 2.2°C or 0.75%
23	HPS-23	TS-RV-1000	TC type K	Outer wall temp. of RV 1000 mm above bottom of melt.	-	0-50 mV	0-1250°C	± 2.2°C or 0.75%
24	HPS-24	TS-RV-mf	TC type K	Temperature of RV middle flange.	-	0-50 mV	0-1250°C	± 2.2°C or 0.75%
25	HPS-25	TS-RV-100	TC type K	Outer wall temp. of RV 100 mm above bottom of melt.	-	0-50 mV	0-1250°C	± 2.2°C or 0.75%
26	HPS-26	TS-RV-bf	TC type K	Temperature of RV bottom flange.	-	0-50 mV	0-1250°C	± 2.2°C or 0.75%
27	HPS-27	TS-vent	TC type E	Outer wall temp. of vent line.	-	0-70 mV	0-900°C	± 1.7°C or 0.5%
28	HPS-28	TF-CT-102	TC type K	Fluid temp. in condensate tank at a water level of 102 mm.	-	0-50 mV	0-1250°C	± 2.2°C or 0.75%
29	HPS-29	TF-CT-406	TC type K	Fluid temp. in condensate tank at a water level of 406 mm.	-	0-50 mV	0-1250°C	± 2.2°C or 0.75%
30	HPS-30	TF-CT-711	TC type K	Fluid temp. in condensate tank at a water level of 711 mm.	-	0-50 mV	0-1250°C	± 2.2°C or 0.75%
31	HPS-31	TF-CT-1016	TC type K	Fluid temp. in condensate tank at a water level of 1016 mm.	-	0-50 mV	0-1250°C	± 2.2°C or 0.75%
32	HPS-32	TF-CT-1321	TC type K	Fluid temp. in condensate tank at a water level of 1321 mm.	-	0-50 mV	0-1250°C	± 2.2°C or 0.75%
33	HPS-33	TF-CT-1626	TC type K	Fluid temp. in condensate tank at a water level of 1626 mm.	-	0-50 mV	0-1250°C	± 2.2°C or 0.75%
34	HPS-34	TF-HX-in	TC type K	Fluid temp. at HX coolant inlet.	-	0-50 mV	0-1250°C	± 2.2°C or 0.75%
35	HPS-35	TF-HX-out	TC type K	Fluid temp. at HX coolant outlet.	-	0-50 mV	0-1250°C	± 2.2°C or 0.75%

Table 2.1 Instrumentation list (part 1 of 2).

#	Channel	Name	Type	Description	Serial #	Output	Range	Accuracy
36	HPQ-51	TF-ST	TC type K	Fluid temp. in spray tank.	-	0-50 mV	0-1250°C	±2.2°C or 0.75%
37	HPQ-53	TG-ST-in	TC type K	Gas temp. in the spray tank line inlet.	-	0-50 mV	0-1250°C	±2.2°C or 0.75%
38	HPQ-54	TG-ST-out	TC type K	Gas temp. in the spray tank line outlet.	-	0-50 mV	0-1250°C	±2.2°C or 0.75%
39	HPS-36	HF-vent	Thermopile	Heat Flux through connecting line to V-ST.	0632	0-5.50 mV	0-5 kW/m^2	±3%
40	HPS-37	I-ign	DC supply	Current supply for thermite ignitor.	-	0-100 mV	0-25 Amps	-
41	HPS-38	TF-quench	TC type K	Temperature of water injected into RV	-	0-50 mV	0-1250°C	±2.2°C or 0.75%
42	HPS-39	Reserve	-	-	-	-	-	-
43	HPS-50	TS-MgO-H50-ϕ50-i	TC type K	Liner temp. 50 mm above bottom of melt, 50 mm from outer wall.	-	0-50 mV	0-1250°C	±2.2°C or 0.75%
44	HPS-51	TS-MgO-H50-ϕ50-o	TC type K	Liner temp. 50 mm above bottom of melt, 20 mm from outer wall.	-	0-50 mV	0-1250°C	±2.2°C or 0.75%
45	HPS-52	TS-MgO-H100-ϕ50-i	TC type K	Liner temp. 100 mm above bottom of melt, 50 mm from outer wall.	-	0-50 mV	0-1250°C	±2.2°C or 0.75%
46	HPS-53	TS-MgO-H100-ϕ50-o	TC type K	Liner temp. 100 mm above bottom of melt, 20 mm from outer wall.	-	0-50 mV	0-1250°C	±2.2°C or 0.75%
47	HPS-54	TS-MgO-H50-ϕ170-i	TC type K	Liner temp. 50 mm above bottom of melt, 50 mm from outer wall.	-	0-50 mV	0-1250°C	±2.2°C or 0.75%
48	HPS-55	TS-MgO-H50-ϕ170-o	TC type K	Liner temp. 50 mm above bottom of melt, 20 mm from outer wall.	-	0-50 mV	0-1250°C	±2.2°C or 0.75%
49	HPS-56	TS-MgO-H100-ϕ170-i	TC type K	Liner temp. 100 mm above bottom of melt, 50 mm from outer wall.	-	0-50 mV	0-1250°C	±2.2°C or 0.75%
50	HPS-57	TS-MgO-H100-ϕ170-o	TC type K	Liner temp. 100 mm above bottom of melt, 20 mm from outer wall.	-	0-50 mV	0-1250°C	±2.2°C or 0.75%
51	HPS-58	TS-MgO-H50-ϕ290-i	TC type K	Liner temp. 50 mm above bottom of melt, 50 mm from outer wall.	-	0-50 mV	0-1250°C	±2.2°C or 0.75%
52	HPS-59	TS-MgO-H50-ϕ290-o	TC type K	Liner temp. 50 mm above bottom of melt, 20 mm from outer wall.	-	0-50 mV	0-1250°C	±2.2°C or 0.75%
53	HPS-60	TS-MgO-H100-ϕ290-i	TC type K	Liner temp. 100 mm above bottom of melt, 50 mm from outer wall.	-	0-50 mV	0-1250°C	±2.2°C or 0.75%
54	HPS-61	TS-MgO-H100-ϕ290-o	TC type K	Liner temp. 100 mm above bottom of melt, 20 mm from outer wall.	-	0-50 mV	0-1250°C	±2.2°C or 0.75%
55	HPS-40	PA-RV	1810AZ	Absolute pressure in reaction vessel.	02351-00P1PM	1-6 V	0-14 bar gage	±0.14 bar
56	HPS-41	PD-CT	1801DZ	ΔP transmitter to measure condensate inventory.	D-9	0-13 V	0-0.35 bar	±0.004 bar
57	HPS-42	L-TDR-CT	BM100A	Time domain reflectometer to measure CT level.	A02331879A	4 - 20 mA	0 - 2 m	±3 mm
58	HPS-43	VDC-P-supply	-	Voltage of the power supply for the pressure transmitters.	-	0 - 15 V	-	-
59	HPQ-50	T-CJ-HPQ	AD592 IC	Cold junction compensation sensor.	-	1μA/K	0-70°C	±0.5°C
60	HPQ-52	TG-CL-out	TC type K	Gas temperature in condensate tank outlet line to spray tank.	-	0-50 mV	0-1250°C	±2.2°C or 0.75%
61	HPQ-55	F-quench	Paddlewheel	Flow rate of water into reaction vessel (for quenching melt).	3144	0-5 V	0-50 gpm	±0.5 gpm
62	HPQ-56	F-HX	Paddlewheel	Flow rate of cold water to heat exchangers.	3143	0-5 V	0-50 gpm	±0.5 gpm

Table 2.2 Instrumentation list (part 2 of 2).

Table 2.3 Remotely operated valves.

Channel #		Valve Name	Type	Description	Actuator
1		V-CT	Ball valve	Valve on steam line between reaction vessel and quench tank.	Pneumatic
2		V-quench	Ball valve	Valve on quench water supply line into reaction vessel.	Solenoid
3		V-quench-i	Ball valve	Isolation valve on quench water supply line into reaction vessel.	Solenoid
4		V-quench-b	Ball valve	Valve on back-up quench water supply.	Solenoid
5		V-ST	Ball valve	Valve on vent line between reaction vessel and spray tank.	Pneumatic
-		V-HX	Ball valve	Valve on cooling-water line to heat exchangers.	Solenoid
-		VC-CT	Ball valve	Control valve on steam line between reaction vessel and quench tank.	Electric

Six C-Type thermocouples were used to measure the temperature at the inner surface of the liner. They were mounted horizontally, passing through fittings in the RV wall and holes drilled through the liner. Each thermocouple is protected by a ? " tantalum sheath. These sensors are used to detect the arrival of the quench front near the melt perimeter. Premature arrival of the front could indicate that water seeps down along the liner and cools the melt from the side, which is undesirable. Though such seepage is deemed unlikely, this must be verified because the dryout heat flux measurement would be compromised by a melt that was partially cooled by water circumventing the crust.

The gap between the liner and the RV wall (see fig. 2.1) was filled with sand in an effort to reduce cooling of the liner and thus lateral heat losses. The concern has been that water can enter the gap and cool the outer surface of the liner through boiling, which would increase lateral heat losses beyond that expected for conduction cooling through the liner and RV wall with natural convection at the RV outer surface. New MgO liners were fabricated for this test and they provide a closer fit within the RV than the previous liners. The gap between the RV wall and liner was less than 5 mm (versus ~10 mm wide for previous tests). Also, instead of filling the gap with sand to the top of the first liner (height of 30 cm), the gap was filled to the top of the second liner.

The entire RV was insulated from the melt level upwards. The lower 25 cm of the RV was left uninsulated so that any excessive wall heating or corium breach could be readily observed.

3. Test Parameters and Course of Test

The specifications for this test are listed in table 3.1 along with those of the first five tests for comparison. The measured masses of the constituents of the corium powder charge are listed in table 3.2. The 68 kg charge was selected to produce an approximate melt depth of 15 cm.

The facility was heated over the course of a couple of hours to bring the structure temperatures up to about 100°C. During this period the water used for melt quenching was preheated to about 95°C. The preheating is used to reduce the amount of energy absorbed by heat sinks in the early stages of the test. This maximizes the amount of steam reaching the heat exchanger and reduces corrections to the measured corium heat flux.

The igniter coil was energized to initiate thermite ignition, which was first detected by a sudden rise in the upper plenum gas temperature TG-RV. Thermocouples within the melt began rising about thirty seconds later. The signal from the igniter has not been included in any graph in this report. All data has been plotted so that the x-axis origin corresponds with the initial rise in TG-RV.

The melt thermocouples within the thermowell (TM-Hm5-ϕ0 through TM-H70-ϕ0) rose rapidly to an initial peak temperature of about 1950°C and then began to slowly fall (some fin-cooling by the thermowell is expected). Figure A.1 shows the first eight minutes of the transient (all plots are attached as an appendix).

Table 3.1 Test specifications for completed SSWICS experiments.

Parameter	Test Number					
	1	**2**	**3**	**4**	**5**	**6**
Test section internal diameter (cm)	30.5	30.5	30.5	30.5	30.5	30.5
Melt composition (wt % UO_2/ZrO_2/Cr/Concrete)	61/25/6/8	61/25/6/8	61/25/6/8	48/20/9/23	56/23/7/14	56/23/6/14
Concrete type	LCS	SIL	LCS	LCS	LCS	SIL
Melt mass (kg)	75	75	75	60	68	68
Melt depth (cm)	15	15	15	15	15	15
Initial Melt Temperature (^oC)	~2300	~2100	~2100	~2100	~2100	~1950
Basemat type	Inert	Inert	Inert	Inert	Inert	Inert
System pressure (bar)	1	1	4	4	4	1
Water injection flowrate (lpm)	4	4	12	13	6	14
Water injected (liters)	33	39	34	40	61	47

Constituent	Mass (kg)
U_3O_8	39.92
CrO_3	8.40
CaO	1.50
Zr	11.68
Mg	0.04
Si	1.08
SiO_2	5.32
Al	0.06
Total	68.0

Tables 3.2 Corium powder charge and reaction product mass fractions.

Constituent	Wt %	
	Reactant	Product
U_3O_8	58.70	-
UO_2	-	56.32
Zr	17.16	-
ZrO_2	-	23.13
Si	1.57	-
SiO_2	7.84	11.17
Mg	0.07	-
MgO	-	0.12
Al	0.09	-
Al_2O_3	-	0.64
CaO	2.21	2.21
CrO_3	12.36	-
Cr	-	6.41

The next phase of the experiment was the initial quench of the melt. Valve V-CT was opened 67 s after ignition so that steam would be able to travel to the heat exchangers. Valve V-ST was closed at 72 s to isolate the vent line and spray tank fom the system. Water injection was initiated at 120 s at an average flow rate of 14 l/min, lasting for 3.5 minutes (ending at 335 s) and resulting in an integrated flow of approximately 47 liters.

The target pressure for the test was 1 bar. Unlike the first two atmospheric pressure tests, the system pressure peaks significantly above 1 bar during the injection phase. The difference is due to the presence of the regulating valve in the steam line, which was installed just prior to SSWICS-3. Even completely open, the valve has enough flow resistance to produce a brief pressurization during the early portion of the transient, when the steam flow rate is very high.

Note that this was the first test in which the steam flow rate (and calculated heat flux) did not fall to zero towards the end of the injection phase. The reason is that, for the first time, the system preheat temperature was equal to the saturation temperature at the selected operating pressure and so relatively little energy was absorbed by the structures. The preheat system was not in place for SSWICS-1&2 and the preheat temperature for subsequent tests was ~100^{o}C for both

structures and injected water (operating pressure and saturation temperature for the latter tests was 4 bar and ~145°C, respectively).

After about four hours of quenching, the thermocouples within the thermowell reached the saturation temperature and the test was terminated.

4. Sensor Malfunctions and Abnormalities

Post test examination of the test apparatus and a preliminary review of the data indicate the following:

1) Sensor TM-H20-ϕ180 failed at some time between 40 s and 275 s after measuring a peak temperature of 2100°C at 32 s.
2) Sensor TIW-H100-ϕ90 failed at 780 s after indicating a much higher temperature than the other TIW TCs. This TC might have protruded from the MgO liner more than the other TCs or the protecting layer of ceramic paste may have fallen away during thermite ignition.
3) TS-MgO-H50-50-i malfunctioned during the entire test.
4) The following auxiliary sensors failed in a fault related to the switchover from the CCI-1 test: T-CJ-HPQ, TF-ST, TG-CL-out, TG-ST-in, TG-ST-out. These sensors are used only for diagnostic purposes and their loss does not influence the usefulness of data obtained from the remaining sensors.

5. Data Reduction

Some simple calculations have been performed to provide a preliminary assessment of the test data. The first is a calculation of the coolant inventory in the RV as a function of time. The inventory is the difference between the total amount of liquid injected and the amount boiled off and collected in the CT:

$$M_{H_2O-RV} = \sum_{t=0}^{t=t_{end}} r\dot{V}\Delta t \quad - \quad \frac{p}{4}D^2\frac{\Delta P}{g} \tag{5.1}$$

where data from sensor F-quench is used for the volumetric flow rate $\dot{V}$ and the liquid density ρ is taken to be 998 kg/m^3. The condensate inventory is calculated with readings from sensor PD-CT (ΔP) and the tank diameter D of 0.203 m. Figure A.9 shows both the integrated mass flow and CT inventory, labeled F-integrated and M-CT, respectively. The calculated net coolant inventory, denoted M-RV, confirms that the corium was always covered with water.

The corium heat flux was calculated using two different methods. The first considers the rate of condensate collection, which is a measure of the steam flow rate from the RV. Accurate determination of the heat flux at the corium surface must, however, account for various heat sinks. During the injection phase, energy is absorbed raising the coolant to the saturation temperature. Some of the vapor produced by the quenching melt condenses on the walls of the upper plenum to heat the RV structures to the saturation temperature. Later, heat losses from the upper plenum generate continued condensation. Accounting for these heat sinks, the rate of energy transfer through the corium surface is written as:

$$Q = M_{RV} c_p \frac{\partial T}{\partial t} + \dot{m} h_{fg} + [M_S c_M \frac{\partial T}{\partial t} + Q_{HL}] \Big|_{up} \quad (5.2)$$

where $\dot{m}$ is mass flow rate of condensate into the CT, M_S is the mass of the RV upper plenum structures, c_M is their heat capacity,, and Q_{HL} represents total upper plenum heat losses. For this report, liquid subcooling has been neglected (an accurate assumption after the injection phase) along with heat losses and time variations in structure temperatures. The condensation rate is calculated from the time derivative of the differential pressure signal PD-CT. The heat transfer rate from the corium is then:

$$Q = \frac{1}{g} \frac{p}{4} D^2 \frac{\partial \Delta P}{\partial t} h_{fg} \quad (5.3)$$

where D is again the inner diameter of the CT and the heat of vaporization h_{fg} is 2130 kJ/kg°C (TG-RV registered 145°C through most of the transient). The heat flux is obtained by scaling Q with the initial surface area of the corium (0.071 m^2). The derivative was calculated with pairs of averaged ΔP readings (an average of 5 measurements at 0.5 Hz) centered around a Δt of 60 s. The averaging and length of Δt were necessary to reduce oscillations in the calculated heat flux.

The second method of calculating corium heat flux uses an energy balance on the secondary side of the heat exchanger. The measured parameters are the coolant flow rate on the secondary side of the cooling coils and the inlet and outlet coolant temperatures. The cooling power of the heat exchanger is then:

$$Q_{HX} = r \dot{V}_{HX} c_p (T_{out} - T_{in}) \quad (5.4)$$

where readings from sensors TF-HX-in and TF-HX-out were used for temperatures T_{in}, and T_{out}, respectively. Data from the flow meter F-HX was used for $\dot{V}_{HX}$ while the density and heat capacity of water were taken to be 982 kg/m^3 and 4.18 kJ/kg°C, respectively.

The cooling power of the heat exchanger is related to the steam flow rate out of the RV by the following:

$$Q_{HX} = \dot{m} [h_{fg} + c_p (T_{sat} - T_{con})] \quad (5.5)$$

where $\dot{m}$ is the mass flow rate of steam into the heat exchanger (identical to the flow rate of condensate into the CT, as defined in equation 5.2). From equation 5.5 it can be seen that if condensate leaves the heat exchanger at the saturation temperature, i.e., there is no subcooling, the cooling power of the heat exchanger is equal to the product of $\dot{m}$ and h_{fg}. In this case, according to equation 5.2, the cooling power of the heat exchanger equals the heat transfer rate from the melt. However, the condensate does not, in general, leave the heat exchanger at the saturation temperature. The result of this subcooling is an overestimation of the corium heat flux when using equation 5.5 and the assumption of $T_{sat} = T_{con}$ (as plotted in figure A.14).

The corium heat flux could be calculated more accurately with the heat exchanger energy balance through the addition of a condensate temperature measurement at the heat exchanger outlet. However, the calculation would still require the steam mass flow rate, which would be derived from the CT level measurements. Thus the heat exchanger energy balance, with the assumption of $T_{sat} = T_{con}$, is considered to be a rough check of the heat flux measurements derived directly from the CT level measurements using equation 5.3.

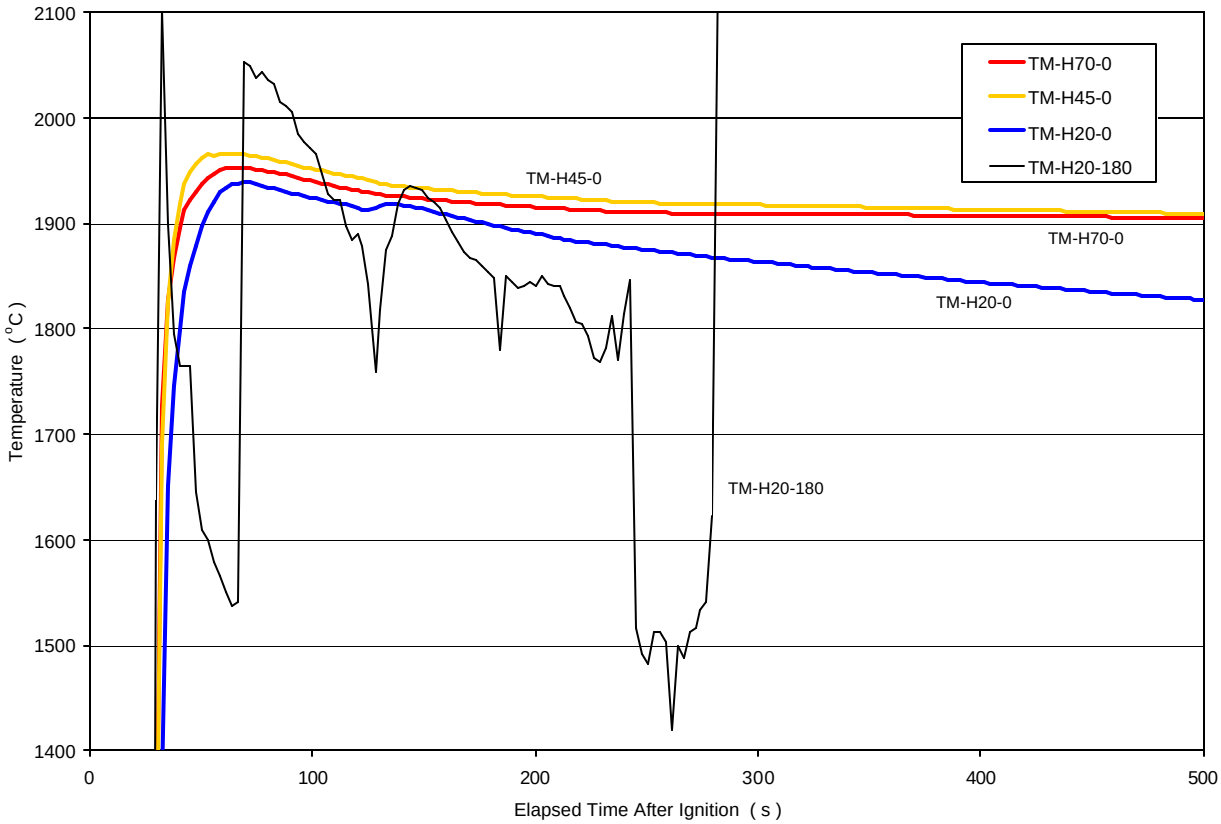

Figure A.1 Melt temperatures early in the transient (H70, H45, and H20-0 in tungsten thermowell).
Figure A.2 Melt temperatures for the entire test duration.

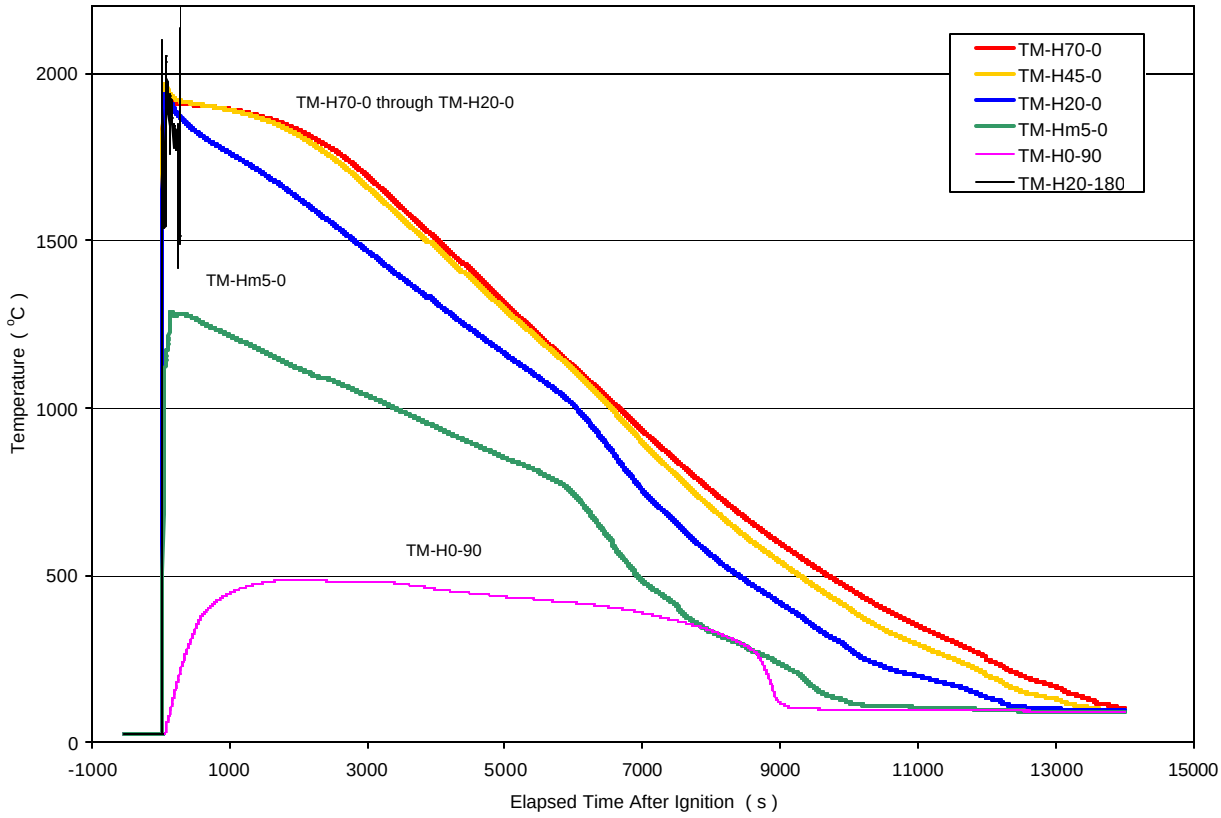

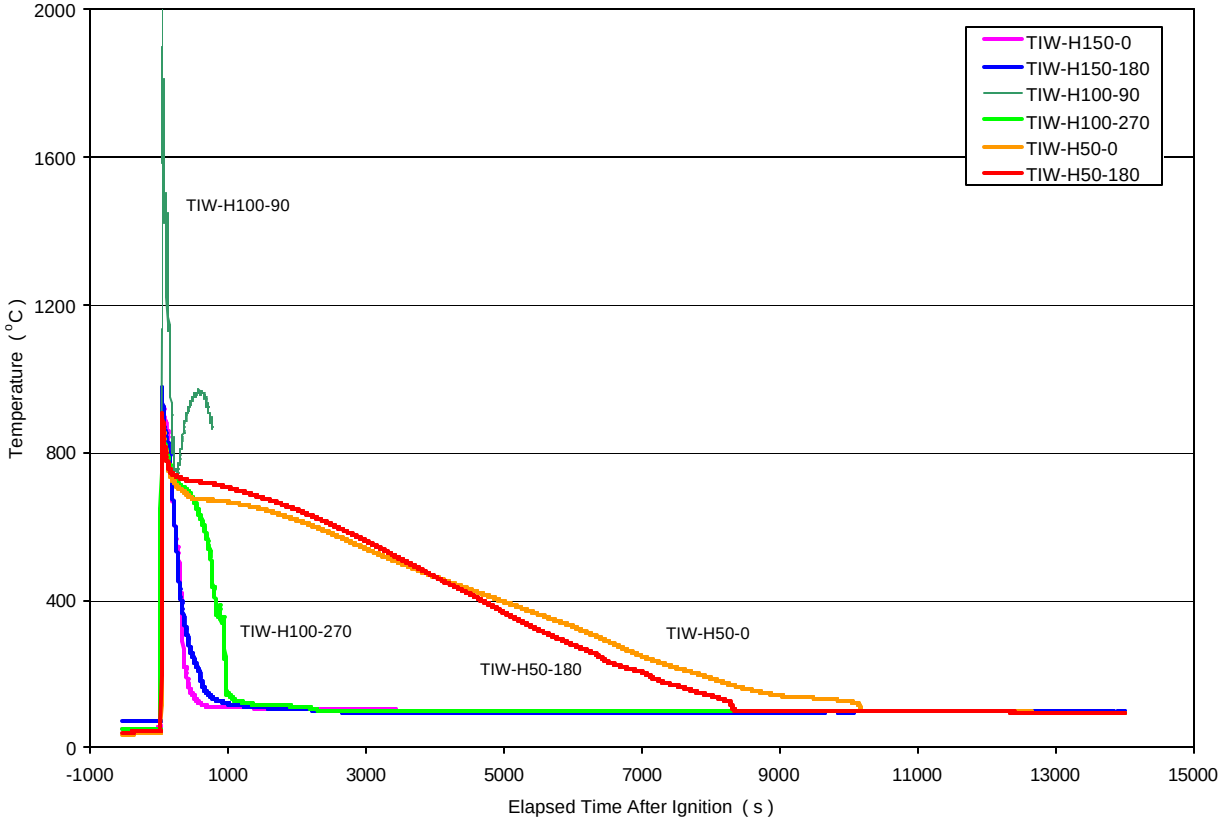

Figure A.3 Temperatures at the inner wall of MgO liner.

Figure A.4 Temperatures within the MgO liner.

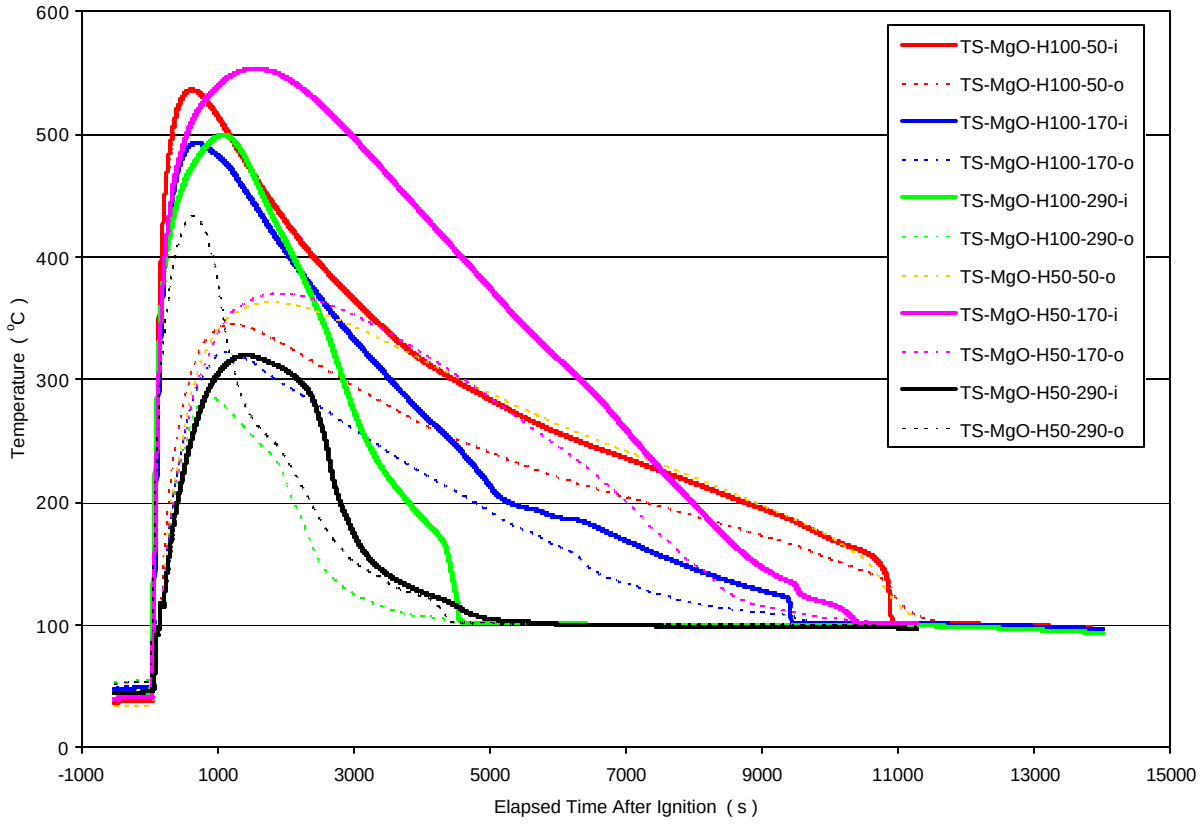

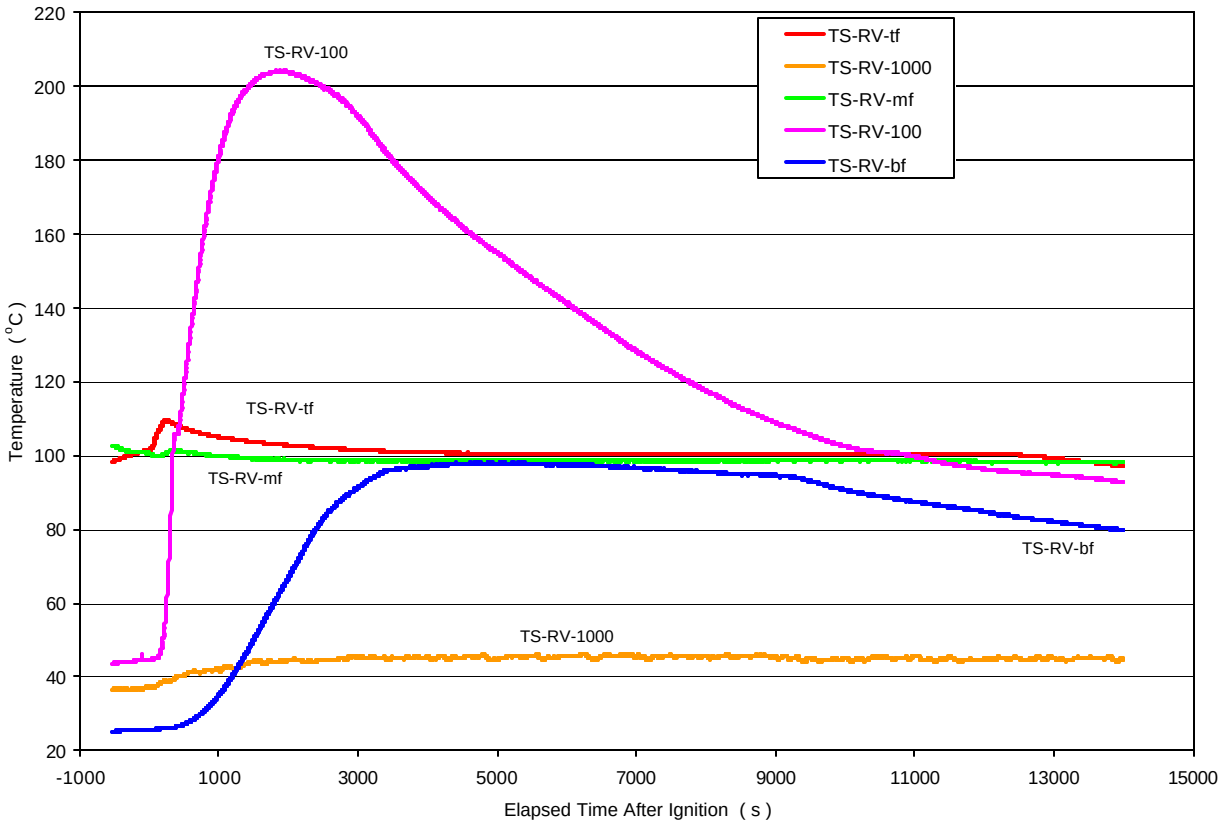

Figure A.5 Temperatures of steel structures.

Figure A.6 Total pressure in reaction vessel and position of valve V-quench.

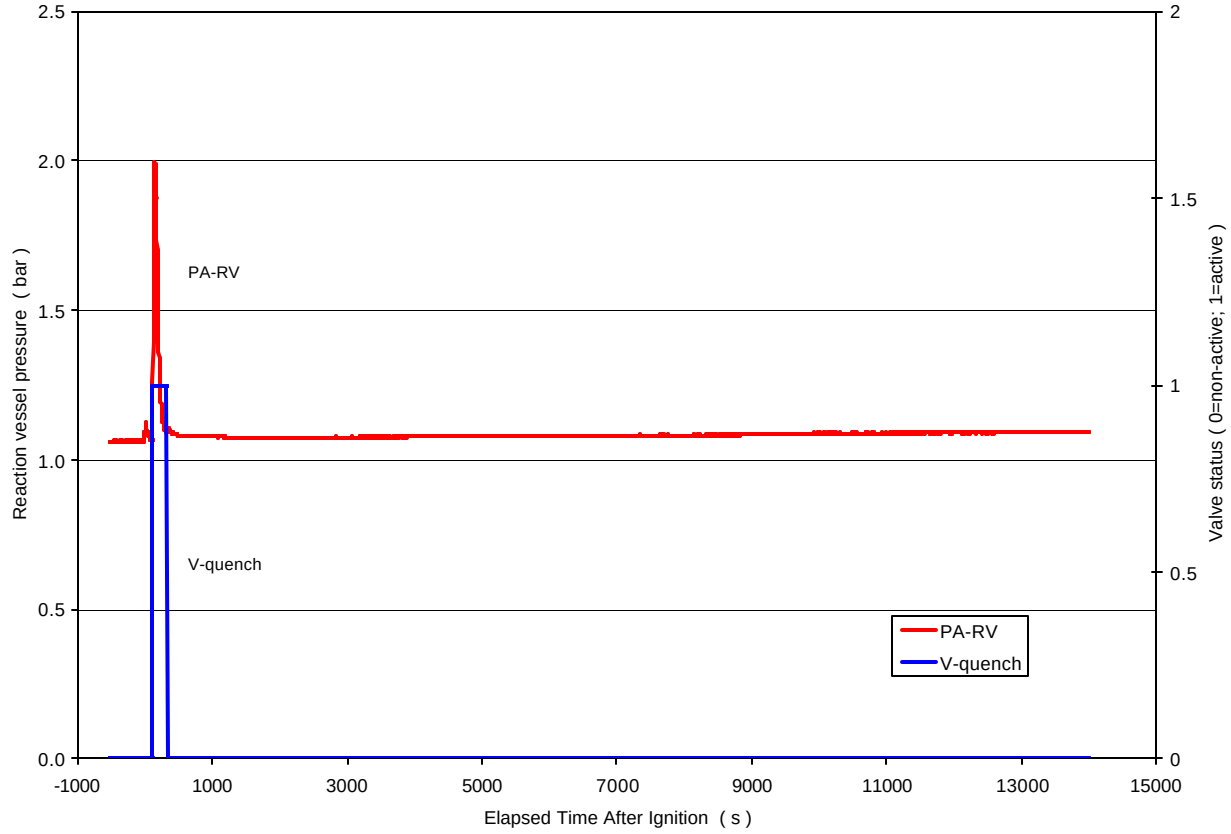

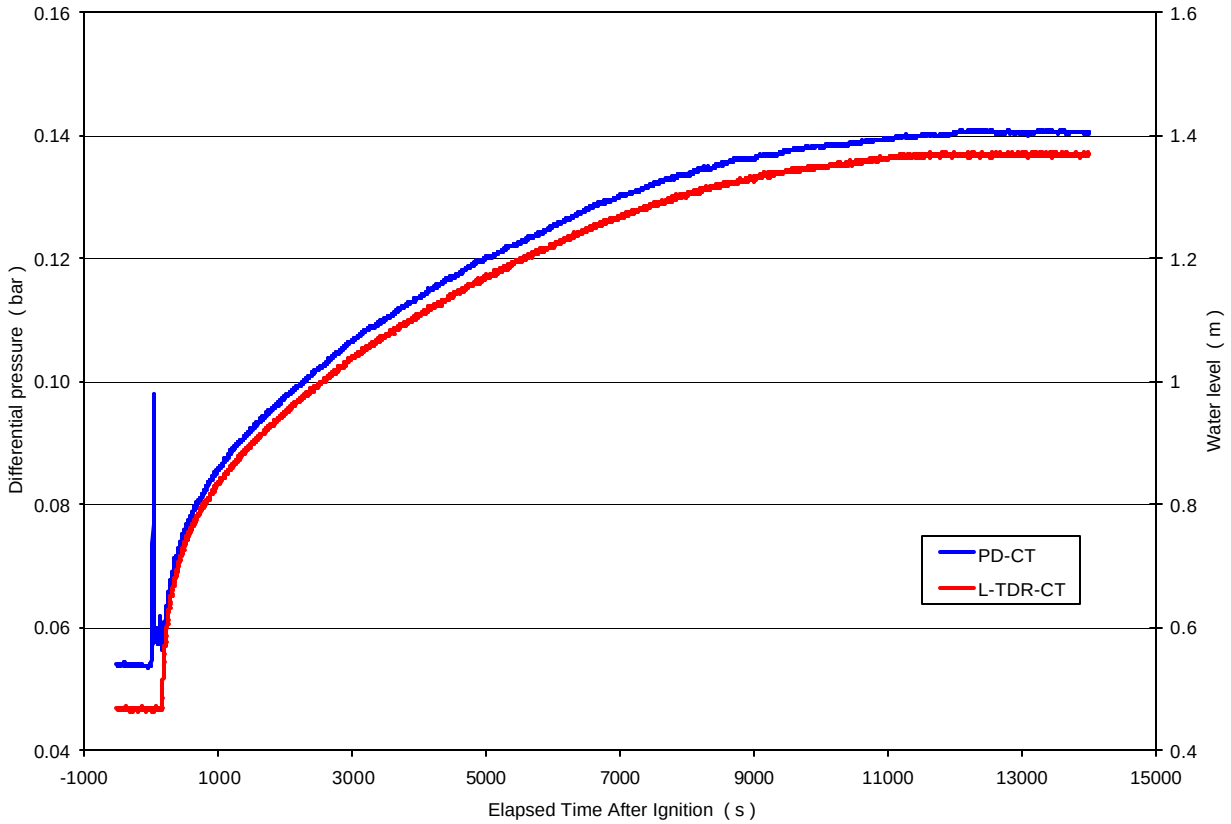

Figure A.7 Condensate tank inventory as measured by DP and level sensors.

Figure A.8 Water injection into RV and HX secondary side flow rate.

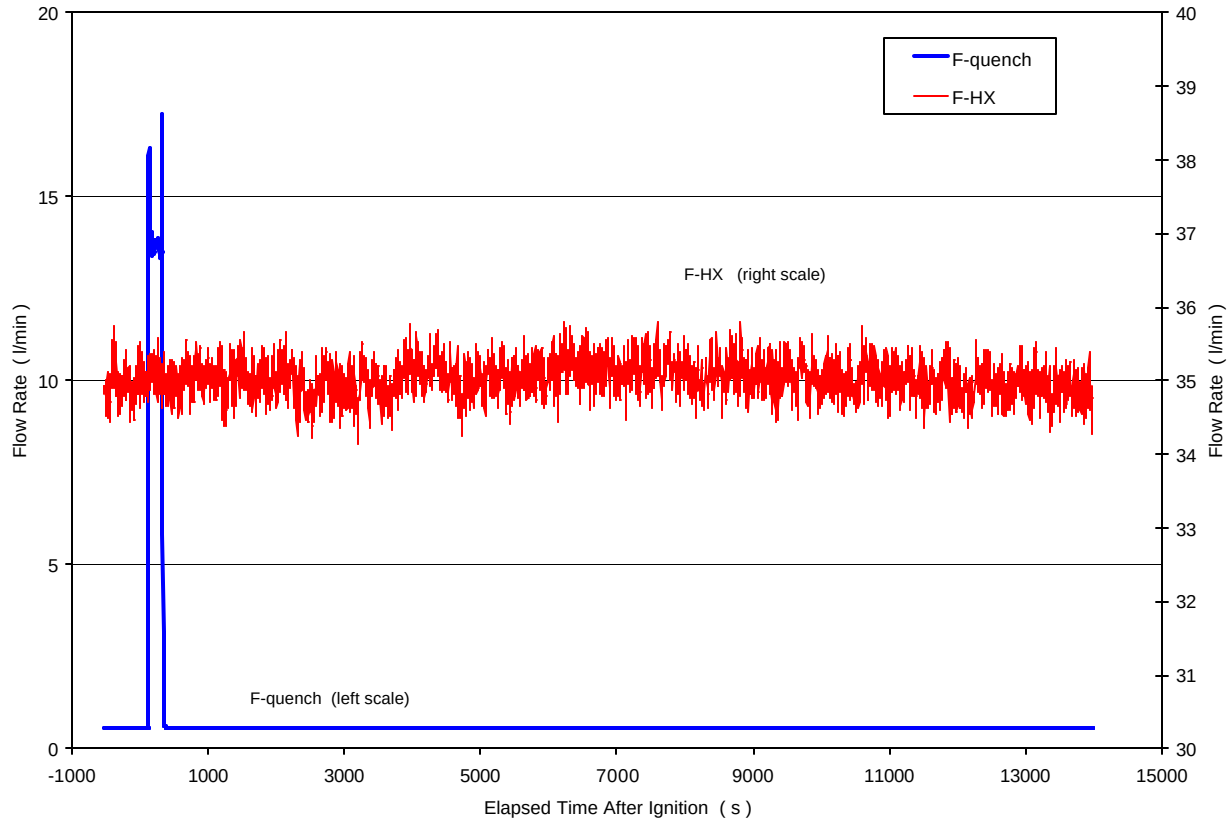

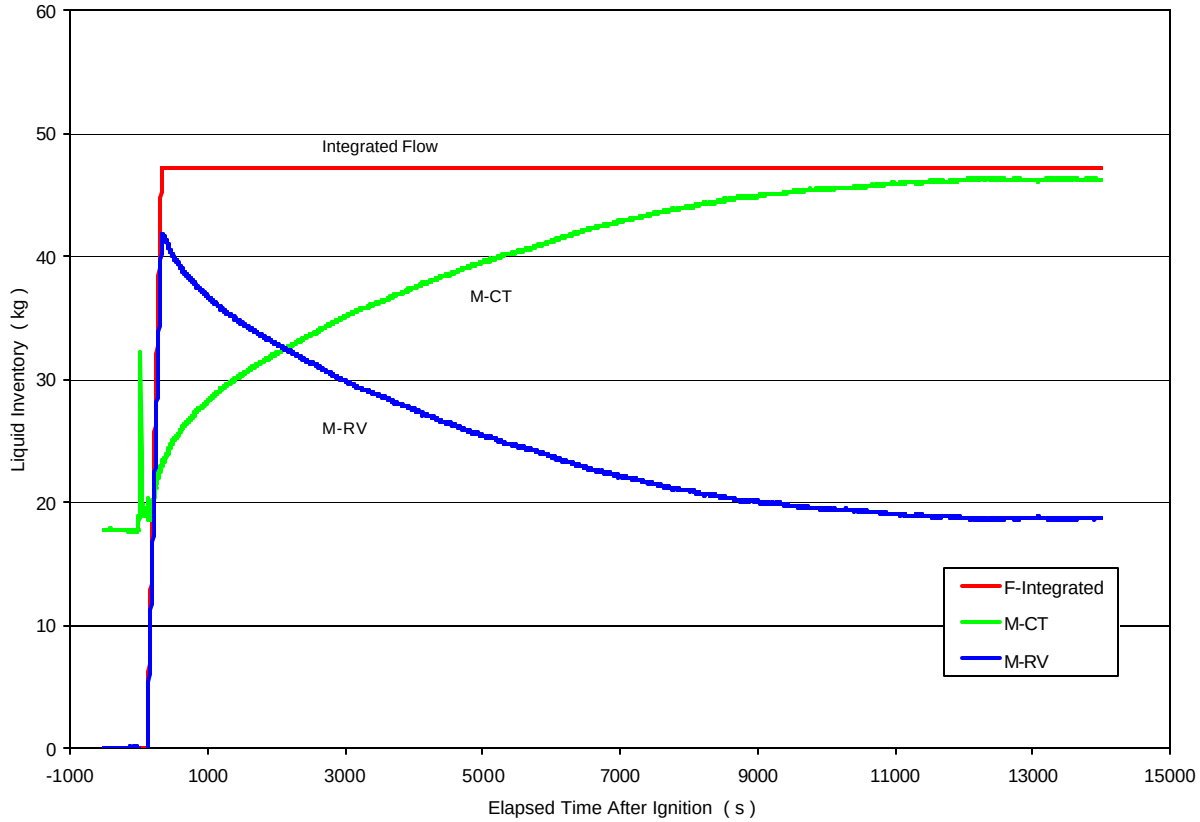

Figure A.9 Integrated quench flow and calculated RV liquid inventory.

Figure A.10 Secondary side fluid temperatures at HX inlet and outlet.

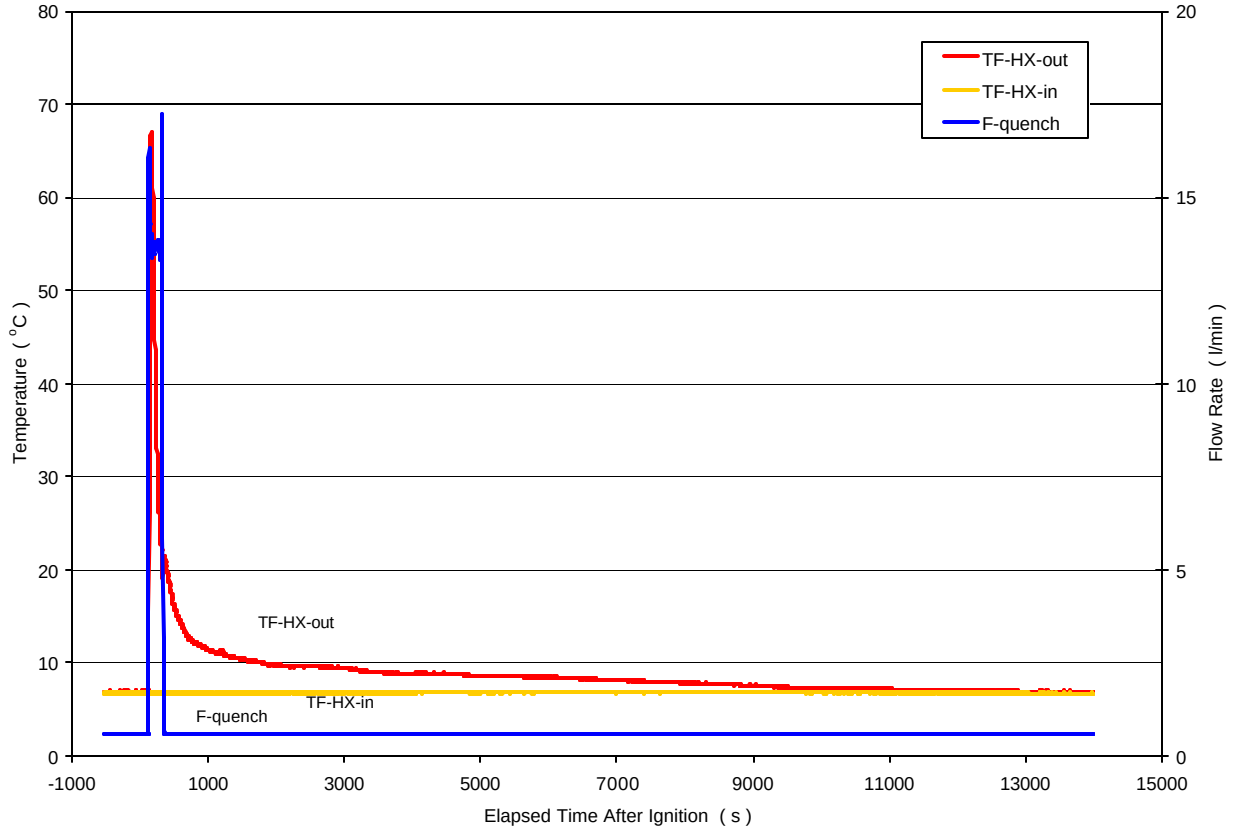

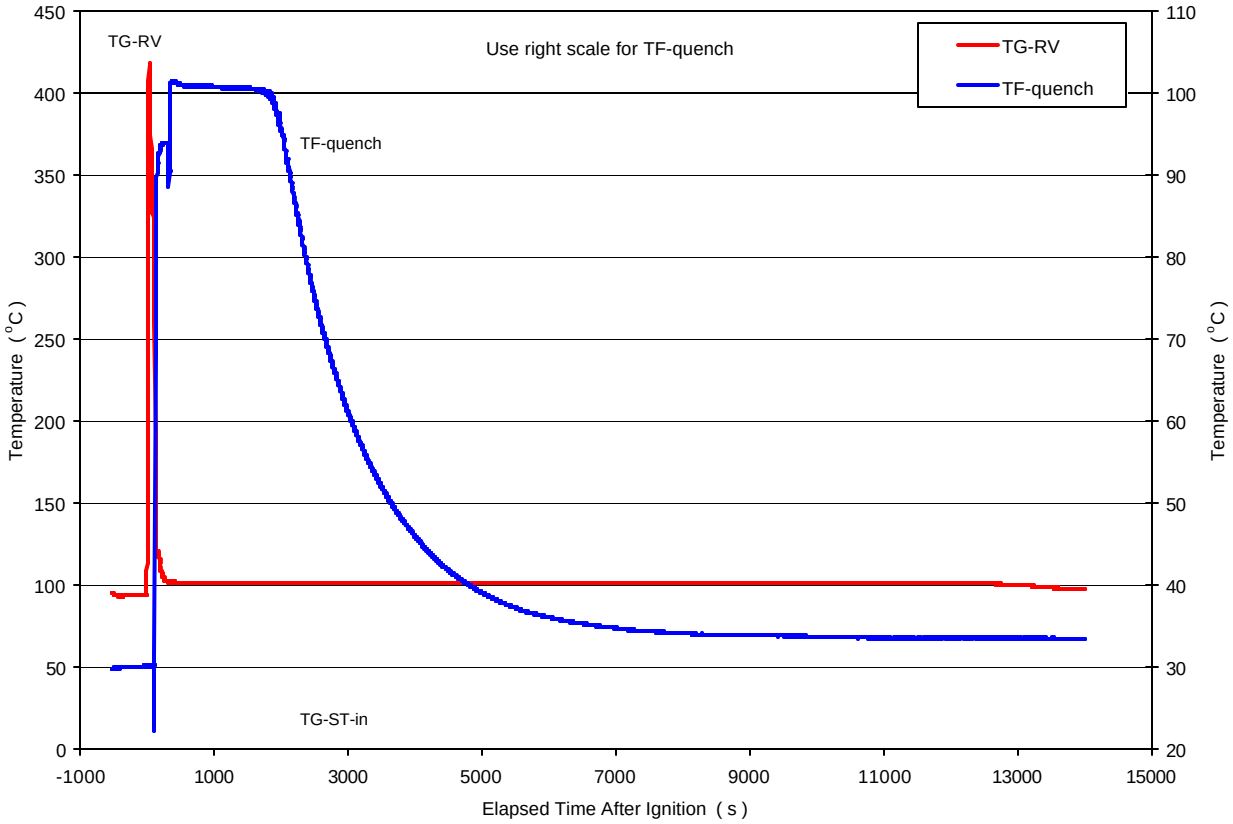

Figure A.11 Miscellaneous gas and fluid temperatures.
Figure A.12 Fluid temperatures in the condensate tank.

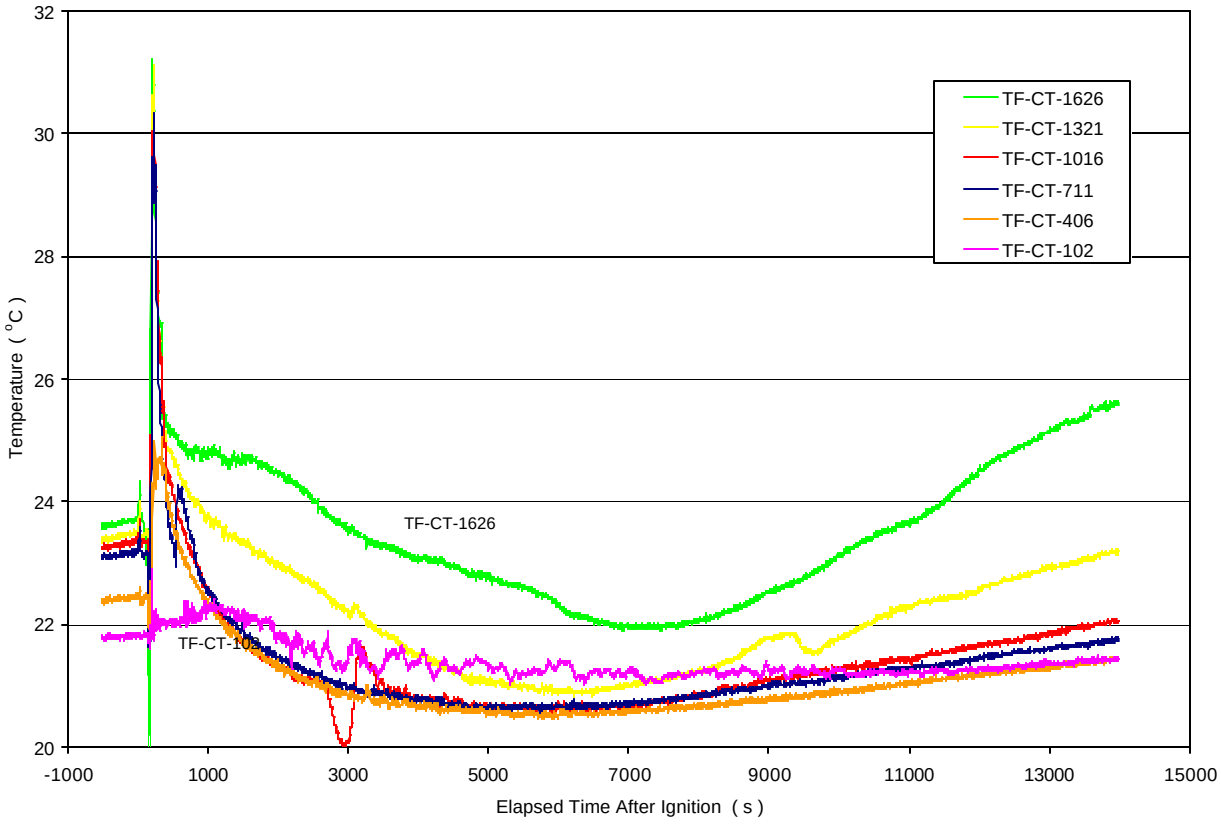

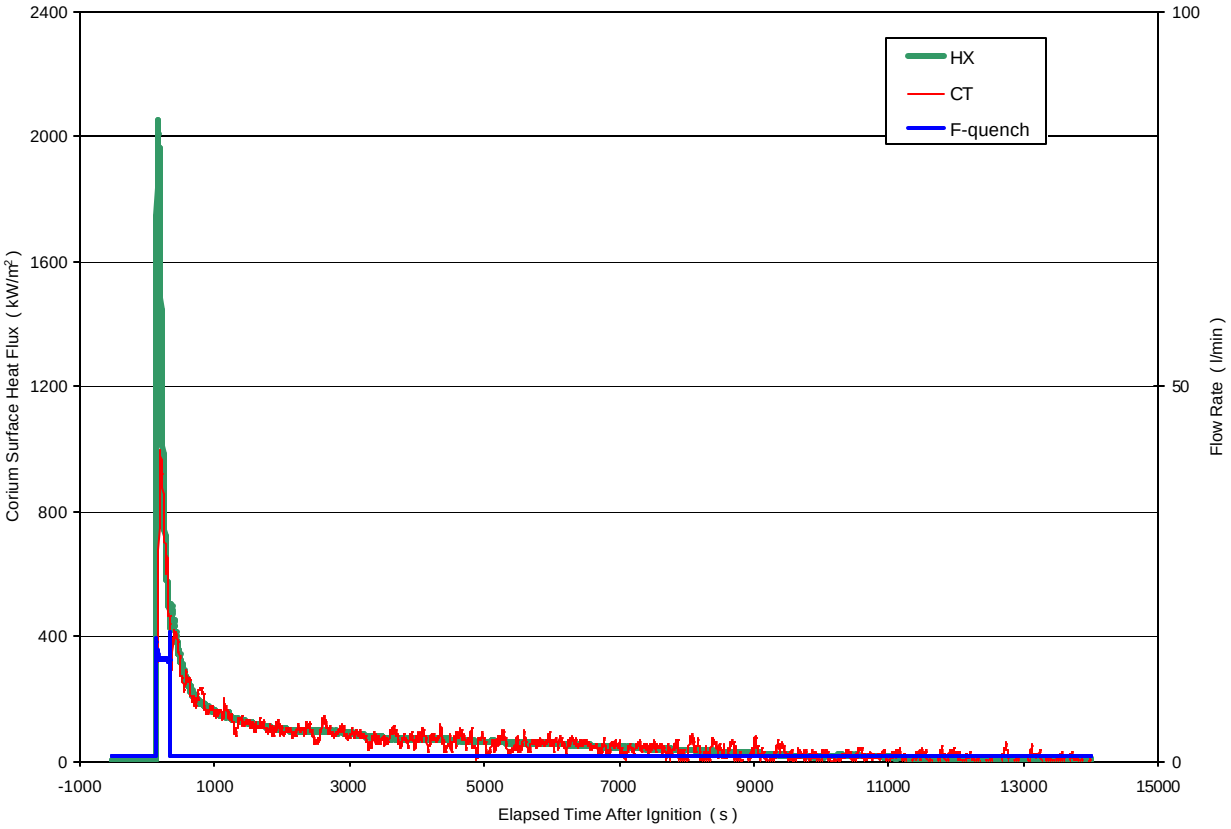

Figure A.13 Energy release from RV, scaled by corium surface area.

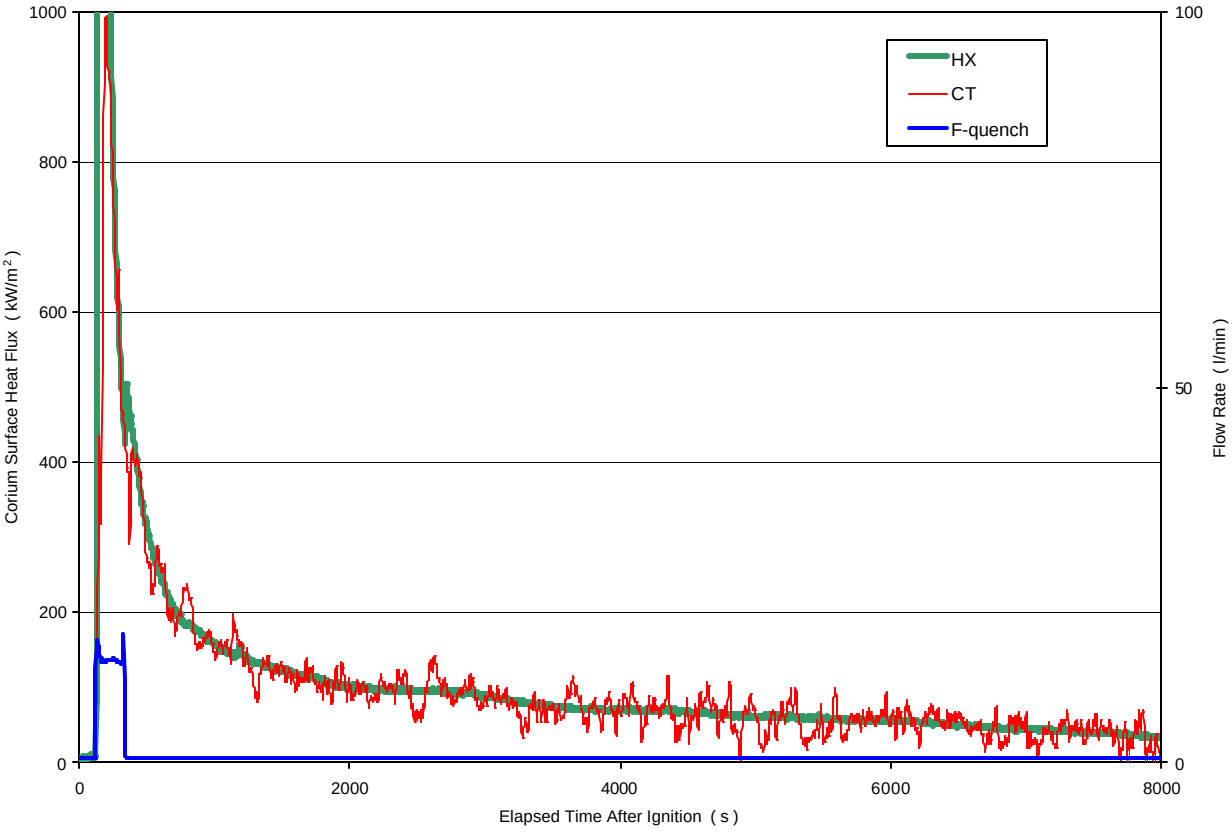

Figure A.14 Energy release from RV, scaled by corium surface area (expanded scale).